

Experimental Results of Image-based Adaptive Visual Servoing of 2D Robots under Jacobian and Dynamic Friction Uncertainties

L.G. García-Valdovinos, E.C. Dean-León, V. Parra-Vega
Mechatronics Division
CINVESTAV-IPN
Av. IPN 2508, Sn P. Zacatenco, México, D.F., C.P. 07300
{lgarcia, edean, vparra}@cinvestav.mx

A. Espinosa-Romero
Faculty of Mathematics
Universidad Autónoma de Yucatán
Mérida, Yucatán, México
eromero@tunku.uady.mx

Abstract—A globally convergent visual feedback control scheme is proposed for dynamical planar robot arms subject to uncertain camera, robot, analytical Jacobian and dynamic friction parameters. When complex friction arises, visual servoing suffers to drive the robot to the desired trajectories, in particular in slow motion and velocity reversals, which are typical motion regime in visual servoing due to the vision system properties. Moreover, dynamic friction is usually neglected in motion control and it is not the exception in visual servoing literature. In order to prove the theory described in this paper, the real-time OS, Linux-RTAI, is used to obtain experimental results of this controller on a direct-drive robot manipulator. Results suggest its excellent performance.

Index Terms— Visual Servoing, Second Order Sliding Mode Control, Adaptive Control, Unknown Jacobian, Dynamic Friction.

I. INTRODUCTION

Dynamic-based visual servoing schemes consider explicitly the robot dynamics, so as to compensate them to achieve a better dynamic response. The obvious advantage of this scheme is the fact that online compensation of uncalibrated camera can be easily carried out along the controller computation. Recently, uncalibrated spatial visual servoing tasks have been proposed using adaptive control for dynamic robot arms to guarantee local tracking subject to parametric uncertainty [1]~[4]. These schemes exploit the fact that the rotation matrix is constant, and formal and rigorous stability analysis support these results. However, this works assume knowledge of the analytical Jacobian matrix, and furthermore, these are singular at rotation angle $\theta = \pi/2$. For planar uncalibrated visual servoing tasks, [4] propose a regulation scheme that removes the requirement of the image Jacobian. Instead, to achieve position tracking, [6] propose a discontinuous first order sliding mode controller. An improvement of this scheme is presented in [7] wherein an excellent combination of adaptive control and second order sliding mode control is used to avoid chattering (introduced by the first order sliding mode) and to overcome the parametric uncertainty of camera, robot and Jacobian. However, none of the papers mentioned before compensate for joint friction. Dynamic friction provokes limit cycles and complex nonlinear behaviors

that may cause instability in mechanical systems [8]. This phenomena deprives to obtain the required precision of a physical system, particularly robot manipulators. Then, joint friction is quite important to compensate because it is a dominant dynamical force in slow and velocity reversal regimes, which is a typical motion regime in robot tasks, and moreover in visual servoing. Thus, the task under study is that the robot end effector tracks a *visual* trajectory, i.e. in image space (see Fig. 1). This task is very relevant in many robotic applications. However, for any practical impact, uncertainties must be considered.

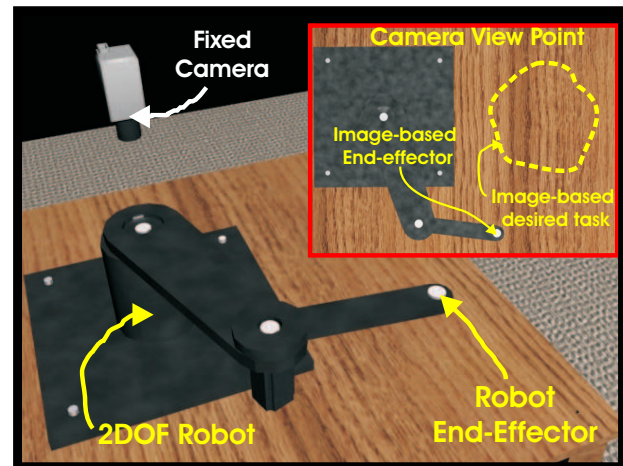


Fig. 1. Experimental Setup.

A. Contribution

In this paper an adaptive second order sliding mode tracking visual feedback controller driven by image errors is developed. It is assumed that camera, robot, Jacobian and dynamic friction parameters are uncertain. As second order sliding mode control does not introduce high frequency signals, it can be implemented in a real plant, unlike the first order sliding mode. Also, as will be seen afterwards, the sliding mode permits to achieve exponential fast convergence of tracking errors. No acceleration is required, and only the visual flow of one landmark is computed.

To illustrate the performance of the proposed controller we present experimental results, that confirms the expected behavior, on a direct-drive robot manipulator.

II. NONLINEAR ROBOT DYNAMICS

The dynamics of a serial n -link rigid, non-redundant, fully actuated robot manipulator can be written as follows

$$H(q)\ddot{q} + C(q, \dot{q})\dot{q} + g(q) = \tau - F(\dot{q}, \dot{z}, z) \quad (1)$$

where $q \in \mathfrak{R}^n$ is the vector of generalized joint displacements, $H(q) \in \mathfrak{R}^{n \times n}$ stands for the symmetric positive definite manipulator inertia matrix, $C(q, \dot{q}) \in \mathfrak{R}^n$ stands for the vector of centripetal and Coriolis torques, $g(q) \in \mathfrak{R}^n$ is the vector of gravitational torques, $F(\dot{q}, \dot{z}, z) \in \mathfrak{R}^n$ is the joint dynamic friction¹ and $\tau \in \mathfrak{R}^n$ stands for the vector of input torque control. Two important properties of robot dynamics, useful for stability analysis, are the following

Property 1: With a proper definition of $C(q, \dot{q})$, $\dot{H}(q) - 2C(q, \dot{q})$ is skew-symmetric. Then

$$X^T \left[\dot{H}(q) - 2C(q, \dot{q}) \right] X = 0, \quad \forall X \in \mathfrak{R}^n \quad (2)$$

Property 2: Robot dynamics are linearly parameterizable in terms of a known regressor $Y_b = Y_b(q, \dot{q}, \ddot{q}) \in \mathfrak{R}^{n \times p}$ and an unknown vector $\theta_b \in \mathfrak{R}^p$ of robot parameters as follows

$$H(q)\ddot{q} + C(q, \dot{q})\dot{q} + g(q) = Y_b\theta_b \quad (3)$$

A. Open loop error equation

Adding and subtracting to (1) the following parametrization

$$H(q)\ddot{q}_r + C(q, \dot{q})\dot{q}_r + g(q) = Y_r\theta_b \quad (4)$$

where the known regressor $Y_r = Y_r(q, \dot{q}, \ddot{q}_r) \in \mathfrak{R}^{n \times p}$ and the unknown constant vector $\theta_b \in \mathfrak{R}^p$, produces the open loop error equation

$$H(q)\dot{S}_q = \tau - C(q, \dot{q})S_q - Y_r\theta_b \quad (5)$$

with joint error surface S_q defined as

$$S_q = \dot{q} - \dot{q}_r \quad (6)$$

where \dot{q}_r stands for the nominal reference of joint velocities, not defined yet.

III. CAMERA MODEL

The static pin hole camera model is used, considering thin lens without aberration [5]. To introduce the model, first consider the robot direct kinematics

$$x_b = f(q) \quad (7)$$

where $x_b \in \mathfrak{R}^n$ represents the position of robot end effector in cartesian space, $q \in \mathfrak{R}^n$ is the vector of generalized joint displacements, and $f(\cdot) : \mathfrak{R}^n \rightarrow \mathfrak{R}^n$. Then, the differential kinematics of robot manipulator, which relates velocities in cartesian space $\dot{x}_b \in \mathfrak{R}^n$ to joint space velocities $\dot{q} \in \mathfrak{R}^n$, is defined as follows

$$\dot{x}_b = J(q)\dot{q} \quad (8)$$

¹For a clear exposition, firstly, $F(\dot{q}, \dot{z}, z)$ will be considered zero, however in Section VII it will be treated.

Now, the visual position $x_s \in \mathfrak{R}^2$ of robot end effector in image space (screen) is given by [5]

$$x_s = \alpha R(\theta) x_b + \beta \quad (9)$$

where α is the scale factor², and $R(\theta) \in SO(3)$, $\beta \in \mathfrak{R}^2$ and depends on intrinsic and extrinsic parameters of camera³. The differential camera model is then

$$\dot{x}_s = \alpha R(\theta) \dot{x}_b \quad (10)$$

where $\dot{x}_s \in \mathfrak{R}^2$ determines the visual robot end effector velocity, i.e. *visual flow*. Notice that the constant transformation $\alpha R(\theta)$ maps statically robot *cartesian velocities* \dot{x}_b into visual flow \dot{x}_s . Using equation (7)~(9), equation (10) becomes

$$\dot{x}_s = \alpha R(\theta) J(q)\dot{q} \quad (11)$$

Thus, the inverse differential kinematics for robot manipulator in terms of visual velocities⁴ becomes

$$\dot{q} = J(q)^{-1} R(\theta)^{-1} \alpha^{-1} \dot{x}_s \Rightarrow \dot{q} = J_{Rinv} \dot{x}_s \quad (12)$$

This relation is useful to design the nominal reference of joint velocities \dot{q}_r in the following section.

IV. DEFINITION OF ERROR MANIFOLDS

According to (12), a nominal reference \dot{q}_r in the joint space is defined as follows

$$\dot{q}_r = J_{Rinv} \dot{x}_r \quad (13)$$

Notice that, we are also interested in designing an image based servo visual force control without computing inverse kinematics⁵, then nominal reference \dot{q}_r must be designed in terms of nominal visual reference. Consider now the next *nominal visual reference* of velocities

$$\dot{x}_r = \dot{x}_{sd} - \alpha \Delta x_s + S_{sd} - \gamma_{s1} \int_{t_0}^t S_{s\delta} - \gamma_{s2} \int_{t_0}^t \text{sign}(S_{s\delta}) \quad (14)$$

where \dot{x}_{sd} stands for desired visual velocity trajectory, $\Delta x_s = x_s - x_{sd}$ is the visual position error, and $\gamma_{si} = \gamma_{si}^T \in \mathfrak{R}_+^{n \times n}$, for $i = 1, 2$. The visual error surface arises

$$S_{s\delta} = S_s - S_{sd} \equiv (\Delta \dot{x}_s + \alpha \Delta x_s) - S_s(t_0) e^{-\kappa_s t}$$

where $\Delta \dot{x}_s = \dot{x}_s - \dot{x}_{sd}$ defines visual velocity error, $\kappa_s > 0$ and $\alpha = \alpha^T \in \mathfrak{R}_+^{n \times n}$. Using equations (12), (13), and (14) into (6), the visual joint error surface arises as follows

$$\begin{aligned} S_q &= \dot{q} - \dot{q}_r \\ &= J_{Rinv} \dot{x}_s - J_{Rinv} \dot{x}_r \\ &= J_{Rinv} S_{vs} \end{aligned} \quad (15)$$

²Without loss of generality, α can be considered as a scalar matrix 2×2 .

³Focal distance, depth of field, translation of camera center to image center, distance between optical axis to the robot base.

⁴With $J_{Rinv} \in \mathfrak{R}^{n \times n}$ whose entries are functions of robot and camera parameters.

⁵To eliminate the inverse kinematics calculus and to reduce the control law computational cost. This is also one byproduct of this scheme.

with

$$S_{vs} = S_{s\delta} + \gamma_{s1} \int_{t_0}^t S_{s\delta} + \gamma_{s2} \int_{t_0}^t \text{sign}(S_{s\delta})$$

where S_{vs} stands for the visual manifold.

Remark 1. The above definition assumes exact knowledge of J_{Rinv} . However, in practice, it stands as a very restricted assumption. Therefore, we need to design an uncertain manifold S_q taking into consideration the uncertainty of J_{Rinv} . To this end, consider

$$\widehat{q}_r = \widehat{J}_{Rinv} \dot{x}_r \quad (16)$$

with \widehat{J}_{Rinv} an estimated of J_{Rinv} , such that $\text{rank } \widehat{J}^{-1}(q)$ and $\widehat{R}_\alpha^{-1}(\theta)$ are full rank $\forall q \in \Omega$, where the robot workspace free of singularities is defined by $\Omega = \{q | \text{rank}(J(q)) = n, \forall q \in \mathbb{R}^n\}$, and $\forall \theta \in \mathbb{R}$. Thus, substituting (16) into (6), we have the *uncalibrated joint error surface*

$$\begin{aligned} \widehat{S}_q &= \dot{q} - \widehat{q}_r \\ &= J_{Rinv} \dot{x}_s - \widehat{J}_{Rinv} \dot{x}_r \end{aligned} \quad (17)$$

where \widehat{S}_q is available because \dot{q} and \widehat{q}_r are available. Adding and subtracting $J_{Rinv} \dot{x}_r$ to (17) we obtain

$$\begin{aligned} \widehat{S}_q &= J_{Rinv} S_{vs} - \Delta J_{Rinv} \dot{x}_r \\ &= S_q - \Delta J_{Rinv} \dot{x}_r \end{aligned} \quad (18)$$

where $\Delta J_{Rinv} = \widehat{J}_{Rinv} - J_{Rinv}$.

V. OPEN LOOP ERROR EQUATION

Using (16), the uncertain parametrization $Y_r \theta_b$ becomes

$$H(q) \widehat{q}_r + C(q, \dot{q}) \widehat{q}_r + g(q) = Y_r \theta_b \quad (19)$$

where $\widehat{q}_r = f(\ddot{x}_r)$, with

$$\ddot{x}_r = \ddot{x}_{sd} - \alpha \Delta \dot{x}_s + \dot{S}_{sd} - \gamma_{s1} S_{s\delta} - \gamma_{s2} \text{sign}(S_{s\delta}) \quad (20)$$

which introduces discontinuous terms. To avoid introducing high frequency discontinuous signals, add and subtract $\tanh(v_s S_{s\delta})$, $v_s > 0$, to \widehat{q}_r , in order to separate continuous and discontinuous signals as follows

$$\widehat{q}_r = \widehat{q}_{rcont} + \gamma_s z_s \quad (21)$$

with $z_s = \tanh(v_s S_{s\delta}) - \text{sign}(S_{s\delta})$. Thus $Y_{cont} = Y_r(q, \dot{q}, \widehat{q}_r, \widehat{q}_{rcont})$ is continuous since $(\widehat{q}_r, \widehat{q}_{rcont}) \in \mathcal{C}^1$, where

$$\widehat{q}_{rcont} = \widehat{J}_{Rinv} \ddot{x}_{rcont} + \widehat{J}_{Rinv} \dot{x}_r$$

with

$$\ddot{x}_{rcont} = \ddot{x}_{sd} - \alpha \Delta \dot{x}_s + \dot{S}_{sd} - \gamma_{s1} S_{s\delta} - \gamma_{s2} \tanh(v_s S_{s\delta}) \quad (22)$$

Therefore (19) becomes

$$H(q) \widehat{q}_r + C(q, \dot{q}) \widehat{q}_r + g(q) = Y_{cont} \theta_b + H \gamma_{s2} z_s \quad (23)$$

Adding and subtracting (23) to (1), we finally obtain the open loop error in function of $(q, \dot{q}, \widehat{q}_r, \widehat{q}_{rcont})$ as follows:

$$H(q) \widehat{S}_q = \tau - C(q, \dot{q}) \widehat{S}_q - Y_{cont} \theta_b - H(q) \gamma_{s2} z_s \quad (24)$$

Now we are ready to present the main result.

VI. CONTROL DESIGN

Theorem 1. Assume that initial conditions and desired trajectories belong to Ω , and consider the robot dynamics (1) in closed loop with the following visual adaptive second order visual servoing control law

$$\tau = -K_d \widehat{S}_q + Y_{cont} \widehat{\theta}_b \quad (25)$$

$$\dot{\widehat{\theta}}_b = -\Gamma Y_{cont}^T \widehat{S}_q \quad (26)$$

where $\Gamma \in \mathbb{R}_+^{p \times p}$ and $K_d \in \mathbb{R}_+^{n \times n}$. If K_d is large enough and error of initial conditions are small enough, and if

$$\gamma_{s2} \geq \left\| \frac{d}{dt} \left\{ R_\alpha(\theta) J(q) \left[\widehat{S}_q + (\Delta J_{Rinv}) \dot{x}_r \right] \right\} \right\|$$

then exponential convergence of visual and force tracking errors is guaranteed.

Proof. The closed loop dynamics between (25)~(26) and (24) yields

$$H(q) \widehat{S}_q = -\{K_d + C(q, \dot{q})\} \widehat{S}_q - Y_{cont} \Delta \theta_b - H(q) \gamma_{s2} z_s \quad (27)$$

$$\Delta \dot{\theta}_b = \Gamma Y_{cont}^T \widehat{S}_q \quad (28)$$

with $\Delta \theta_b = \theta_b - \widehat{\theta}_b$. The proof is organized in two parts.

Part I. Boundedness of Closed Loop Trajectories.

Consider the time derivative of the following *Lyapunov* candidate function

$$V = \frac{1}{2} \left[\widehat{S}_q^T H(q) \widehat{S}_q + \Delta \theta_b^T \Gamma^{-1} \Delta \theta_b \right] \quad (29)$$

along the solutions of (27)-(28) as

$$\dot{V} \leq -\widehat{S}_q^T K_d \widehat{S}_q + \|\widehat{S}_q\| \psi \quad (30)$$

where Property 1 has been used, and $|\gamma_{s2}| |H(q)| |z_s| \leq \psi$, for $\psi > 0$ is a constant. Now if K_d is large enough and the initial errors are small enough, we conclude the seminegative definiteness of (30) outside of hyperball $\varepsilon_0 = \{\widehat{S}_q | \dot{V} \geq 0\}$ centered at the origin, such that the following properties of the state of closed loop system arise

$$\widehat{S}_q \in \mathcal{L}_\infty \rightarrow \|S_{vs}\| \in \mathcal{L}_\infty \quad (31)$$

Then, $(S_{s\delta}, \int \text{sign}(S_{s\delta})) \in \mathcal{L}_\infty$, and since desired trajectories are C^2 and feedback gains are bounded, we have that $(\widehat{q}_r, \widehat{q}_{rcont}) \in \mathcal{L}_\infty$. The right hand side of (24) shows that $\varepsilon_1 > 0$ exists such that

$$\|\widehat{S}_q\| \leq \varepsilon_1$$

This result shows global stability of \widehat{S}_q and \widehat{S}_q . Now we prove that the sliding modes arises. Rewriting (18)

$$\widehat{S}_q = J_{Rinv} S_{vs} - \Delta J_{Rinv} \dot{x}_r \quad (32)$$

Since $\widehat{S}_q \in \mathcal{L}_2$, and J_{Rinv} is bounded, then $J_{Rinv} S_{vs}$ is bounded. Now, taking into account that \widehat{S}_q is bounded, then $\frac{d}{dt} J_{Rinv} S_{vs}$ is bounded. All this chains of conclusions proves that there exists a constant $\varepsilon_2 > 0$ such that

$$\left| \dot{S}_{vs} \right| < \varepsilon_2$$

Now, we have to prove that for a proper selection of feedback gains γ_{s1} , γ_{s2} , trajectories of visual position converges to zero. This is possible if we can prove that sliding modes are established in the visual position space.

Part II: Second Order Sliding Mode. If we multiply (18) by $R_\alpha(\theta) J(q)^6$, we have

$$R_\alpha(\theta) J(q) \hat{S}_q = S_{s\delta} + \gamma_{s1} \int_{t_0}^t S_{s\delta} + \gamma_{s2} \int_{t_0}^t \text{sign}(S_{s\delta}) - R_\alpha(\theta) J(q) \{\Delta J_{Rinv} \dot{x}_r\} \quad (33)$$

Taking the time derivative of (33), and multiplying it by $S_{s\delta}^T$ produces

$$\begin{aligned} S_{s\delta}^T \dot{S}_{s\delta} &= -\gamma_{s2} S_{s\delta}^T \text{sign}(S_{s\delta}) - \gamma_{s1} S_{s\delta}^T S_{s\delta} + \\ & S_{s\delta}^T \frac{d}{dt} \left[R_\alpha(\theta) J(q) \left(\hat{S}_q + \Delta J_{Rinv} \dot{x}_r \right) \right] \\ & \leq -\mu_s |S_{s\delta}| - \gamma_{s1} \|S_{s\delta}\|^2 \end{aligned} \quad (34)$$

where $\mu_s = \gamma_{s2} - \varepsilon_4$, and $\varepsilon_4 = \frac{d}{dt} \left[R_\alpha(\theta) J(q) \left(\hat{S}_q + \Delta J_{Rinv} \dot{x}_r \right) \right]$, and $\gamma_{s1} > 0$. Thus, we obtain the sliding condition if $\gamma_{s2} > \varepsilon_4$, such that $\mu_s > 0$ of (34) guarantees the sliding mode at $S_{s\delta} = 0$ at $t_s = \frac{|S_{s\delta}(t_0)|}{\mu_s}$. Notice that for any initial condition $S_{s\delta}(t_0) = 0$, then $t_s = 0$, which implies that the sliding mode at $S_{s\delta}(t) = 0$ is guaranteed for all time [13]. This implies the global exponential convergence of image-based tracking errors with smooth control effort

$$S_{s\delta} = 0 \forall t \rightarrow S_s = S_{sd} \rightarrow \Delta \dot{x} = -\alpha \Delta x + S_s(t_0) e^{-\kappa_s t}$$

Remark 2. How to tune feedback gain: γ_{s2} . Since γ_{s2} depends on the norm of the derivative of the state it is difficult to know *a priori* its value to induce a sliding mode. Suppose γ_{s2} is set to zero, in which case our controller renders asymptotic stability. Constant γ_{s2} can be increased gradually until sliding modes arise. Note that this is not a high gain result since larger γ_{s2} do not mean a larger domain of stability. Nevertheless, γ_{s2} is small because the outer adaptive control loop compensates for disturbances.

Remark 3. Well-posed Jacobian: Apparently there is problem with $J(q(t))^{-1}$. However, we have proved that $J(q(t))$ is not singular for all time, because $q(t) \rightarrow q_d(t)$ exponentially, without overshoot, with desired trajectories belonging to robot workspace Ω , thus $J(q(t)) \rightarrow J(q_d(t))$ within Ω and $J(q(t))^{-1}$ is well-posed $\forall t$.

VII. DYNAMIC FRICTION COMPENSATION

The following *LuGre* [8] dynamic friction model is considered

$$\begin{aligned} F(\dot{q}, \dot{z}, z) &= \sigma_0 z + \sigma_1 \dot{z} + \sigma_2 \dot{q} \\ \dot{z} &= -\sigma_0 h(\dot{q}) z + \dot{q} \\ h(\dot{q}) &= \frac{|\dot{q}|}{\alpha_0 + \alpha_1 \exp^{-(\dot{q}/\dot{q}_s)^2}} \end{aligned} \quad (35)$$

where matrix parameters $\sigma_1, \sigma_2, \sigma_3$ are diagonal definite matrices $n \times n$, the state $z \in \mathbb{R}^n$ stands for the position of the bristles, $\alpha_0, \alpha_1 > 0$, and $\dot{q}_s > 0$. This model exhibits

⁶Remember the equality: $J_{Rinv} = J^{-1}(q) R_\alpha^{-1}(\theta)$.

the following complex dynamic friction effects (see [8] for more details on this model).

- Backlash.
- Viscous friction.
- Stiction and static friction.
- Stribeck effect.
- Elastic and plastic deformation.
- Pre-sliding regime.

These effects involve a very complex dynamics around the trivial equilibrium, and for bidirectional motion, and for very small displacements, the forces that comes out from this model makes impossible to reach the origin due to the limit cycles induced and the potentially unstable behavior. Substituting (35) into (1) yields

$$H(q) \ddot{q} + C(q, \dot{q}) \dot{q} + \sigma_{12} \dot{q} + g(q) + \sigma_0 z - \sigma_{01} h(\dot{q}) z = \tau \quad (36)$$

where $\sigma_{01} = \sigma_0 \sigma_1$ and $\sigma_{12} = \sigma_1 + \sigma_2$. Substituting the uncalibrated nominal reference (16) in (36), just like (19), lies the next equation

$$H(q) \hat{\ddot{q}} + C(q, \dot{q}) \hat{\dot{q}} + \sigma_{12} \hat{\dot{q}} + g(q) + \sigma_0 z - \sigma_{01} \hat{h}(\dot{q}) z = \tau \quad (37)$$

Similar to [9], only the part of the equation (37) that is linear in parameters (LP) is rewritten in terms of the uncalibrated nominal reference $(\hat{q}_r, \hat{\dot{q}}_r)^T \in \mathbb{R}^{2n}$ as follows

$$H(q) \hat{\dot{q}}_r + C(q, \dot{q}) \hat{\dot{q}}_r + \sigma_{12} \hat{\dot{q}}_r + g(q) = Y_r \hat{\Theta}_b + \sigma_{12} \hat{\dot{q}}_r \quad (38)$$

Notice that $Y_r \theta_b \neq Y_r \Theta_b$. To be able to cast the problem of non-LP of equation (35) as a disturbance rejection problem, [9] proposes a discontinuous virtual regressor, which in turn yields chattering, with harmful consequences to real physical systems. To avoid chattering the following virtual *continuous* regressor is introduced

$$\frac{\sigma_{01} \alpha_{01}}{\alpha_0} |\dot{q}| \tanh(\xi_f \hat{S}_q) + \sigma_0 \alpha_{01} \tanh(\xi_f \hat{S}_q) = Y_f \Theta_f, \quad (39)$$

where $\alpha_{01} = \alpha_0 + \alpha_1$, $\tanh(q)$ is the continuous hyperbolic tangent function, and $\xi_f > 0$. If we add and subtract (38) and (39) to (36), the following parametrization arises

$$H(q) \hat{\ddot{S}}_q + C(q, \dot{q}) \hat{\dot{S}}_q + \sigma_{12} \hat{\dot{S}}_q = \tau - \mathcal{F} - Y \hat{\Theta} - H(q) \gamma_s z_s \quad (40)$$

with

$$\begin{aligned} \mathcal{F} &= \sigma_0 \left\{ z + \alpha_{01} \tanh(\xi_f \hat{S}_q) \right. \\ & \quad \left. + \alpha_0^{-1} \sigma_1 \alpha_{01} |\dot{q}| \tanh(\xi_f \hat{S}_q) \right. \\ & \quad \left. - \sigma_1 |\dot{q}| z (\alpha_0 + \alpha_1 \exp^{-(\dot{q}/\dot{q}_s)^2})^{-1} \right\} \end{aligned} \quad (41)$$

where $Y = [Y_r, Y_f]$, and $\hat{\Theta} = [\hat{\Theta}_b^T, \Theta_f^T]^T$. Finally, solving (40) for $H(q) \hat{\ddot{S}}_q$, yields the following open-loop visual error dynamics subject to dynamic friction and robot parametric uncertainties

$$H(q) \hat{\ddot{S}}_q = -C(q, \dot{q}) \hat{\dot{S}}_q - \sigma_{12} \hat{\dot{S}}_q + \tau - \mathcal{F} - Y \hat{\Theta} - H(q) \gamma_s z_s \quad (42)$$

Finally, consider the following visual adaptive force-position control law

$$\tau = -K_d \hat{S}_q + Y \hat{\Theta} \quad (43)$$

$$\hat{\Theta} = -\Gamma Y^T \hat{S}_q \quad (44)$$

where $\Gamma \in \mathbb{R}_+^{p \times p}$, $K_d \in \mathbb{R}_+^{n \times n}$. We now have the following result.

Theorem 2 Assume that initial conditions and desired trajectories belong to Ω , and consider the controller (43)-(44). If K_d is large enough and a error of initial conditions are small enough, and if

$$\gamma_{s2} \geq \left\| \frac{d}{dt} \left\{ R_\alpha(\theta) J(q) \left[\hat{S}_q + \Delta J_{Rinv} \dot{x}_r \right] \right\} \right\|$$

then exponential convergence of visual tracking errors is guaranteed.

Proof: With the very same Lyapunov function of *Theorem 1*, we obtain the following time derivative, along trajectories of the closed loop of (43)-(44) and (42),

$$\dot{V} \leq -\hat{S}_q^T K_d \hat{S}_q + \|\hat{S}_q\| \psi - \dot{V}_f \quad (45)$$

where

$$\begin{aligned} \dot{V}_f &= \sigma_0 \hat{S}_q^T [z + \sigma_{01} \tanh(\xi_f \hat{S}_q)] - \sigma_{01} \hat{S}_q [-zh(\dot{x}) \\ &+ \alpha_0^{-1} \sigma_{01} |\dot{x}| \tanh(\xi_f \hat{S}_q)]. \end{aligned} \quad (46)$$

In [11], [12] it was proved that $\dot{V}_f > 0$, and $|\dot{V}_f| < \varepsilon_4$, $\varepsilon_4 > 0$. Then, \dot{V}_f is positive definite outside the hyperball $\rho_0 = \rho_0(\hat{S}_q) = \left\{ \hat{S}_q | V_f \leq 0 \right\}$ with $\|\rho_0\| \leq \rho$, for $\rho > 0$. Thus, if we choose ξ_f large enough, preventing that the mechatronic system does not introduce high frequency from the term $\tanh(\xi_f \hat{S}_q)$, then (45) becomes

$$\dot{V} \leq -\hat{S}_q^T K_f \hat{S}_q + \|\hat{S}_q\| \psi + \rho. \quad (47)$$

where $|\gamma_s| |H(q)| |z_s| \leq \psi$, for $\psi > 0$ is a constant. Then, if K_d is large enough and the initial errors are small enough, we conclude the seminegative definiteness of (30) outside of hyperball $\varepsilon_0 = \left\{ \hat{S}_q | \dot{V} \geq 0 \right\}$ centered at the origin. Afterwards, we proceed exactly as in proof of theorem 1 (part I and part II), and it is therefore omitted. **QED.**

Remark 4. Important properties of this control scheme have to be highlighted: Is an Image-based dynamical control scheme that presents, for first time in literature, compensation of dynamic friction, based on visual information feedback.

VIII. EXPERIMENTAL STATION

Robot parameters and constant gains used in the experiments are shown in Table I, and an image of the experimental setup is depicted in Fig. 2.

TABLE I
DIMENSION PARAMETERS (*Par*) OF THE ROBOT ARM, AND FEEDBACK GAINS.

Par	Value	Gain	Value
m_1	6.72 Kg	K_d	$diag(20, 1.65)$
m_2	2.03 Kg	γ_1	$diag(0.1)$
l_1	0.4 m	α	$diag(5)$
l_2	0.3 m	Γ	$diag(0.001)$

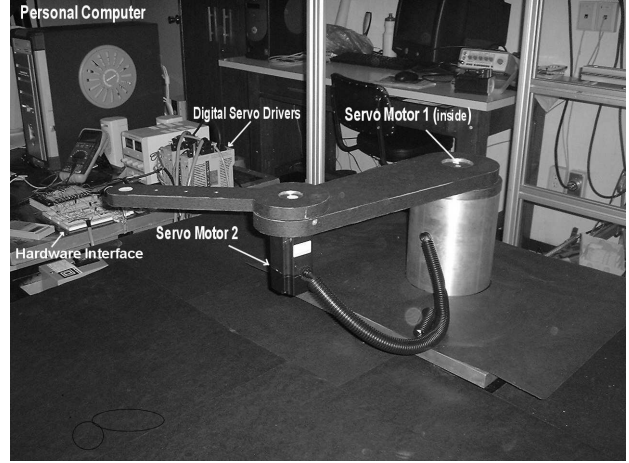


Fig. 2. The two-link planar arm.

A. The Hardware

Direct-drive Yaskawa AC servomotors SGM-08A314 and SGM-04U3B4L with 2048 pulse encoders are directly coupled to the links of the 2-dof arm. Digital drive electronics from the Yaskawa servopacks (SGD-08AS and SGDA-04AS) are integrated, as shown in Fig. 2. The fixed camera used is the SONY DFW-V500 CCD.

B. The firmware and software

The control system is running on a 2.2 GHz PC over Linux-RTAI operating system. The control is composed by two real time parallel processes. The first process sets communication with the SONY DFW-V500 camera via IEEE1394 protocol and controls the acquisition of the robot end effector position in image space. This process runs with sampling rate of 30 Hz. The second process, computes the torque output for the servopacks and runs with a sampling rate of 1 KHz. Communication between process is done by shared memory allocation. Low level programming provides the interface to a Sensoray 626 I/O card which contains internal quadrature encoder interface, 14 bit resolution analog outputs and digital I/O. Velocity is computed using a dirty Euler numerical differentiation formula filtered with a lowpass second order Butterworth filter, with a cutoff frequency of 20Hz.

IX. EXPERIMENTAL RESULTS

The robot is initialized with a high gain PD since the parametric uncertainty is 100%. The inertial frame of the whole system is at the base of the robot. The

end effector is requested to draw a circle in the cartesian space (transformed into image space) centered in (0.55,-0.0) degrees, with a radius of 0.1 m and with an $\omega = 0.628$ rad/s (the circle is done in 10 seconds). The experiment lasts 30 seconds.

A. Results

Fig. 3 depicts the robot performance in image space and visual tracking errors. Notice the exponentially fast convergence of visual tracking errors to the minimum error that can be achieved: 1 pixel. Fig. 4 shows the real and desired tracking in joint coordinates. Finally, Fig. 5 shows input torques. It can be observed that there are not saturation problems and the smooth behavior.

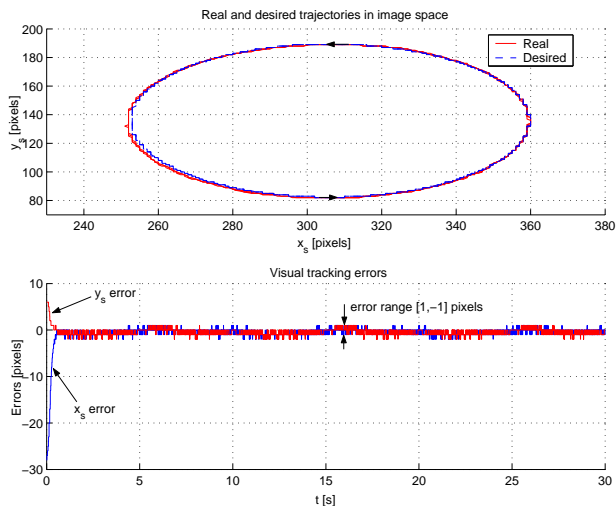


Fig. 3. Task in image space and visual tracking errors.

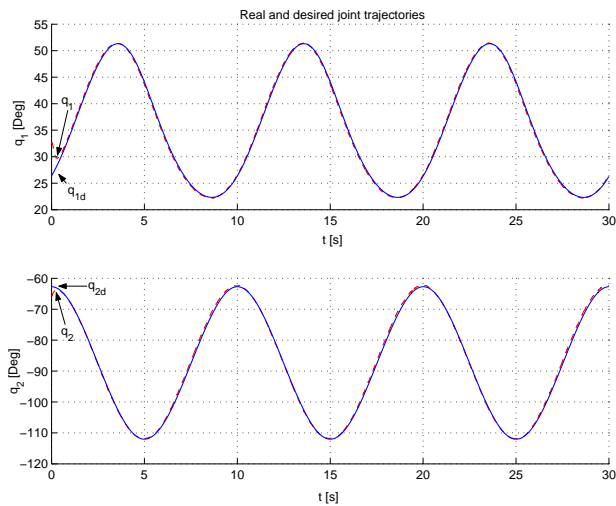


Fig. 4. Joint tracking (real and desired).

X. CONCLUSIONS

A fast trajectory tracking and smooth controller is experimentally validated. The adaptive controller is designed over a second order sliding mode error coordinate system

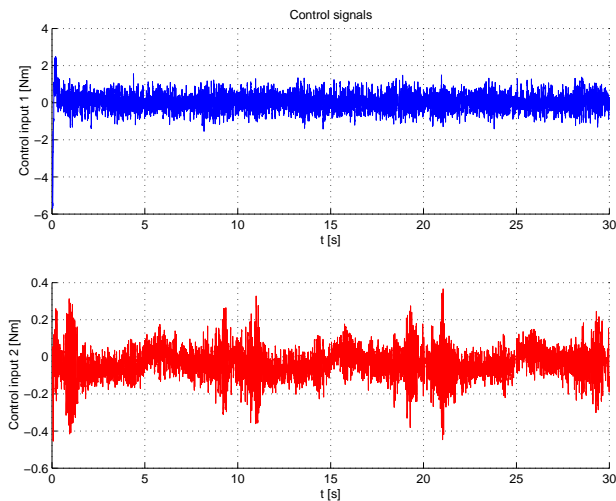


Fig. 5. Applied torques.

to attain exponential convergence, and enhanced parameter stability. Exponential convergence arises for image-based position even when the robot parameters, camera parameters, and analytical Jacobian are considered unknown. Additionally, it is proposed a compensator of uncertain dynamic friction, which is usually neglected in visual servoing, but it is of particularly concern in visual motion tasks, because the motion regime is slow with velocity reversals. Experimental results validate the predicted theoretical performance.

ACKNOWLEDGMENTS

L. Garcia and E. Dean thank CONACYT support under a doctoral scholarship #158613 and #158973. V. Parra-Vega acknowledges support from CONACYT project number 39727-Y.

REFERENCES

- [1] Hsu, L., and Aquino, P., "Adaptive Visual Tracking with Uncertain Manipulator Dynamics and Uncalibrated Camera," Proc. 38th IEEE Conference on Decision and Control, pp. 1248-1253, Phoenix, USA, 1999.
- [2] Bishop, B.E., and M.W. Spong, "Adaptive Calibration and Control of 2D Monocular Visual Servo Systems," IFAC Symp. on Robot Control, Nantes, France, 1997.
- [3] W.E Dixon, E. Zergeroglu, Y. Fang, and D.M. Dawson, "Object Tracking by a Robot Manipulator: Robust Cooperative Visual Servoing Approach," Proc. IEEE Intl. Conf. on Rob. and Autom., pp. 211-216, Washington, USA, 2002.
- [4] Y. Shen, G. Xiang, Y.H. Liu and K. Li, "Uncalibrated Visual Servoing of Planar Robots," Proc. IEEE Int. Conf. on Rob. and Autom., pp. 580-585, Washington, USA, 2002.
- [5] S. Hutchinson, G. Hager, P. C., "A tutorial on visual servo control," IEEE Trans. on Robotics and Automation, Vol. 6, pp. 651-670, 1996.
- [6] V. Parra-Vega, J.D. Fierro-Rojas and A. Espinosa-Romero, "Uncalibrated Sliding Mode Visual Servoing of Uncertain Robot Manipulators," IEEE/RSJ Int. Conf. on Intelligent Robots and Systems, Lausanne, Switzerland, 2002.
- [7] V. Parra-Vega, J.D. Fierro-Rojas and A. Espinosa-Romero, "Adaptive Sliding Mode Uncalibrated Visual Servoing for Finite-time Tracking of 2D Robot," IEEE Int. Conf. on Rob. and Autom., pp. 3048-3054, Taipei, Taiwan, 2003.
- [8] Canudas de Wit, C., Olsson, H., and Astrom, K.J., "A New Model for Control of Systems with Friction," IEEE Transactions of Automatic Control, Vol. 40., No. 3, 419-425, 1995.

- [9] Panteley, E., Ortega, R., and Gafvert, M., "An Adaptive Friction Compensator for Global Tracking in Robot Manipulators," *Systems and Control Letters*, Vol. 33, No. 5, 307 - 313, 1998.
- [10] L.G. García-Valdovinos, V. Parra-Vega, "Experimental Issues of Finite Time Compensation of Dynamic Friction for Robots," *Proc. American Control Conference*, Denver, USA, 2003.
- [11] Parra-Vega, V., Adaptive compensation of dynamic friction in finite time of 1 DOF mechanical system. *American Control Conference*, 2001. *Proceedings of the 2001*, Volume: 3, 25-27 June 2001, pp: 2462 - 2467 vol.3
- [12] García-Valdovinos, L. G., *Seguimiento Perfecto en Tiempo Finito de Robots Manipuladores Sujetos a Fricción Dinámica*, Master Thesis, Dept of EE, Mechatronics Division, CINVESTAV-IPN, México, D.F., 2003.
- [13] Utkin, V., "Variable Structure Systems: Control and Optimisation," MIR, 1993.